

# Threshold phenomenology of nucleon form factors

Rinaldo Baldini Ferroli<sup>1</sup> Simone Pacetti<sup>2</sup> Egle Tomasi-Gustafsson<sup>3</sup>

<sup>1</sup> Laboratori Nazionali di Frascati dell'INFN, Frascati, 00044, Italy

<sup>2</sup> Dipartimento di Fisica e Geologia e Sezione INFN, Perugia, 06123, Italy

<sup>3</sup> CEA, IRFU, SPhN, Saclay, Gif-sur-Yvette Cedex, 91191, France

**Abstract:** The complete knowledge of nucleon form factors is a mandatory pass to deeply understand the dynamics of strong interaction at regimes where QCD is still non perturbative. Phenomenology, i.e., the description of the data by means models based of first principles and depending on physical quantities, represents one of the most powerful tools to attain such a degree of knowledge.

**Key words:** Nucleon form factors, analyticity, threshold behavior, asymptotic behavior

**PACS:** 13.40.Gp, 11.55.Fv, 11.10.Jj

## 1 Definition and basic properties

### 1.1 Definitions

The nucleon form factors [1] (FFs) parametrize the factor to be associated to the photon-nucleon-antinucleon vertex, see fig. 1,  $\gamma N\bar{N}$ , assuming extended nucleons, i.e., particles with non-pointlike charge and magnetic moment spatial distributions.

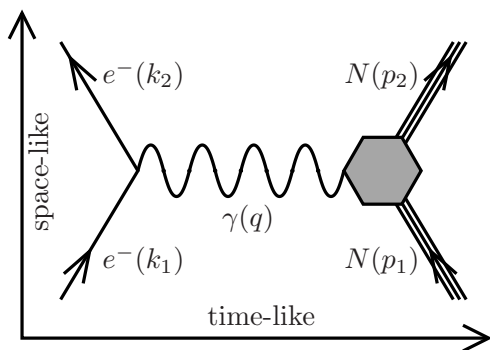


Fig. 1. Feynman diagram of the one-photon exchange annihilation and scattering processes  $e^+e^- \rightarrow N\bar{N}$  and  $e^-N \rightarrow e^-N$ . The hexagon represents the non-pointlike nucleon vertex.

The Feynman amplitude of diagram in fig. 1, in the space-like direction, i.e., for the scattering process, reads

$$\mathcal{M} = \frac{1}{q^2} e\bar{u}(k_2)\gamma_\mu u(k_1) e\bar{U}(p_1)\Gamma^\mu(p_1, p_2)U(p_2),$$

where  $-e$  is the electron charge,  $u$  and  $U$  are the spinors of electrons and nucleons respectively, and the four-momenta, in parentheses, are defined as in fig. 1. The

non-constant matrix,  $\Gamma^\mu(p_1, p_2)$ , which describes the nucleon vertex is

$$\Gamma^\mu(p_1, p_2) = \gamma^\mu F_1^N(q^2) + \frac{i\sigma^{\mu\nu}q_\nu}{2M_N} F_2^N(q^2), \quad (1)$$

where  $F_1^N$  and  $F_2^N$  are the Dirac and Pauli FFs. Such an expression represents the most general Lorentz four-vector, containing gamma matrices and nucleon four-momenta, that fulfills Lorentz, parity, time-reversal and gauge invariance. Form factors are scalar Lorentz functions of  $q^2$ , where  $q$  is the photon four-momentum.

### 1.2 Analyticity

The hexagon in fig. 1 symbolizes the sum of all the electromagnetic contributions, i.e., all those diagrams having an arbitrary number of loops of all hadrons (computable in scalar quantum electrodynamics), with the only: photon, nucleon and antinucleon external lines. The amplitudes of all these diagrams are analytic functions in the whole  $q^2$  complex plane, except for a discontinuity cut, along the positive real axis, starting from  $q_0^2 = (2M_\pi)^2$ . Such a threshold corresponds to the mass of the lightest hadronic state that can couple with the virtual photon. Moreover, the hermiticity of the electromagnetic current operator of the nucleons implies the Schwarz reflection principle for FFs. So that, they are real for real  $q^2$  outside the cut, while they have non vanishing imaginary parts for real  $q^2 > (2M_\pi)^2$ .

Received 14 Sep. 2014

1) E-mail: rinaldo.baldini@lnf.infn.it

2) E-mail: simone.pacetti@pg.infn.it

3) E-mail: egle.tomasi@cea.fr

### 1.3 Sachs form factors

From the expression of the nucleon electromagnetic four-current in terms of the Dirac and Pauli FFs,

$$J_N^\mu = e\bar{U}(p_1)\Gamma^\mu(p_1, p_2)U(p_2) \\ = e\left(F_1^N + \frac{q^2}{4M_N^2}F_2^N, \bar{U}(p_1)\vec{\gamma}U(p_2)(F_1^N + F_2^N)\right),$$

another pair of FFs can be defined as

$$G_E^N(q^2) = F_1^N(q^2) + \tau F_2^N(q^2), \\ G_M^N(q^2) = F_1^N(q^2) + F_2^N(q^2), \quad \tau = \frac{q^2}{4M_N^2}. \quad (2)$$

These are the Sachs electric and magnetic FFs [2], that, in the Breit frame, where the nucleon four-momenta are  $p_1 = (E, -\vec{q}/2)$  and  $p_2 = (E, \vec{q}/2)$ , represent the Fourier transforms of the nucleon charge and magnetization spatial distributions. It follows that their values at  $q^2 = 0$  correspond to the total charge,  $Q_N$ , and magnetic moment,  $\mu_N$ , of the nucleon, i.e.,  $G_E^N(0) = Q_N$ ,  $G_M^N(0) = \mu_N$ .

### 1.4 Measuring form factors

The differential cross section for the elastic scattering, in Born approximation, Feynman diagram of fig. 1 in vertical direction, and in the laboratory frame (Lab), also known as Rosenbluth formula [3], reads

$$\frac{d\sigma_{eN}}{d\Omega} = \frac{\alpha^2\omega_2\cos^2\left(\frac{\theta_e}{2}\right)}{4\omega_1^3\sin^4\left(\frac{\theta_e}{2}\right)}\frac{1}{1-\tau}\left\{G_E^N(q^2) \right. \\ \left. - \tau\left[1+2(1-\tau)\tan^2\left(\frac{\theta_e}{2}\right)\right]G_M^N(q^2)\right\}, \quad (3)$$

while the annihilation cross section, in the same approximation, but in the  $e^+e^-$  center of mass frame (CoM), is [4]

$$\frac{d\sigma_{N\bar{N}}}{d\Omega} = \frac{\alpha^2\beta}{4q^2}\mathcal{C}\left[\frac{1}{\tau}\sin^2(\theta)|G_E^N(q^2)|^2 \right. \\ \left. + (1+\cos^2(\theta))|G_M^N(q^2)|^2\right], \quad \beta = \sqrt{1-\frac{1}{\tau}}, \quad (4)$$

where  $\theta_e$ ,  $\omega_{1,2}$  are the scattering angle, the initial and final energies of the electron in Lab,  $\mathcal{C}$  is the Coulomb correction,  $\theta$  is the scattering angle and  $\beta$  the velocity of the outgoing proton in CoM.

By studying the angular distributions of the scattering and annihilation processes, Sachs FFs can be measured: completely in the space-like region,  $q^2 < 0$ , where they are real; only in modulus in the time-like region,  $q^2 > 0$ , above the physical threshold  $q_1^2 = (2M_N)^2$ , where they

are complex. Moreover, by using only cross section data, the time-like complex structure of FFs remains inaccessible, as well as their values below the threshold  $q_1^2$ , in the so-called unphysical region,  $0 \leq q^2 \leq q_1^2$ .

Besides this procedure, FFs can also be measured by using polarization observables, i.e., by exploiting the so-called Akhiezer-Rekalo polarization method [5]. In particular, the polarization transferred to the nucleon, initially unpolarized, by longitudinally polarized electrons in a scattering process, allows to measure space-like FFs. More in detail, by exploiting of the scattering process  $e^-p \rightarrow e^-p^\uparrow$  (the up-arrow stands for polarization), the ratio between the transversal (in the scattering plane) and the longitudinal component of the outgoing proton polarization vector in Lab is proportional to the ratio of FFs [5], i.e.,

$$\frac{P_T^p(q^2)}{P_L^p(q^2)} = -\frac{2M_p \cot(\theta_e/2)}{\omega_1 + \omega_2} \frac{G_E^p(q^2)}{G_M^p(q^2)},$$

where the symbols are those of eq. (3).

In the annihilation process  $e^+e^- \rightarrow N^\uparrow\bar{N}^\uparrow$ , due to the complex nature of time-like FFs, unpolarized electrons produce polarized nucleons. In particular, the component, orthogonal to the scattering plane, of the nucleon polarization vector in CoM is [6]

$$P_\perp^N(q^2) = \frac{-\sqrt{\tau}\sin(2\theta)\left|\frac{G_E^N(q^2)}{G_M^N(q^2)}\right|}{\tau(1+\cos^2(\theta)) + \sin^2(\theta)\left|\frac{G_E^N(q^2)}{G_M^N(q^2)}\right|^2}\sin(\Phi^N),$$

where symbols follow the labelling of eq. (4) and  $\Phi^N$  is the relative phase between electric and magnetic FFs. It follows that, by detecting the polarization of only one of the final nucleons, the phase of the complex ratio  $G_E^N/G_M^N$  can be measured.

### 1.5 Basic properties

The complex nature of the amplitude and hence of FFs, for time-like values of  $q$ , which is expressed formally by the optical theorem, relies in the fact that the photon, with such a four-momentum, gets enough virtual mass,  $\sqrt{q^2}$ , to couple with, and hence produce a series of on-shell hadronic intermediate states. Besides multi hadron ones, light vector meson resonances are the strongest coupled, i.e., the most probable intermediate states. They represent the main contributions to the FFs even though, having masses below the physical threshold  $\sqrt{q_1^2}$ , their peaks lie in the unphysical region. The complex structure of a prototype FF  $F(q^2)$  is sketched in fig. 2, where the three-dimensional surface (grid) represents the modulus squared  $|F(q^2)|^2$  versus the unphysical  $q^2$  complex plane. Indeed, it is in this Riemann sheet,

\*The , the position of the pole in the  $q^2$  complex plane is strictly connected to the physical mass and width of the resonance, the definition of such quantities depends on the function used to describe the cross section. For instance, by using the relativistic Breit-Wigner

where analyticity can be violated, that a generic resonance, of mass  $M_j$  and width  $\Gamma_j$ , manifests itself as a pair of complex conjugate poles  $z_j$  and  $z_j^*$  (this is due to the Schwarz reflection principles), with  $z_j \simeq M_j^2 + i\Gamma_j M_j^*$ .

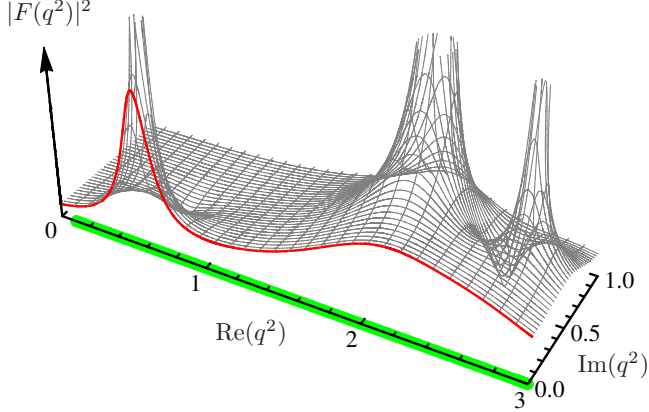


Fig. 2. Pictorial representation of first quarter of the  $q^2$  unphysical complex plane. The grid surface represents the modulus squared of a prototype FF  $F(q^2)$ . The poles are the resonances, the red curve is the  $|F(q^2)|^2$  as it appears for real values of  $q^2$ , i.e., it is the intersection between the surface and the plane  $\text{Im}(q^2) = 0$ . The green band indicates the discontinuity cut  $((2M_\pi)^2, \infty)$ .

## 1.6 The asymptotic behavior

The space-like asymptotic behavior of FFs is inferred by means of dimensional counting rules of quantum chromodynamics [7]. At high space-like  $q^2$ , i.e.  $q^2 \ll -\Lambda_{\text{QCD}}^2$ , the momentum transferred by the virtual photon to the nucleon must be shared among the constituent quarks, in order for the nucleon to remain intact, by gluon exchanges.

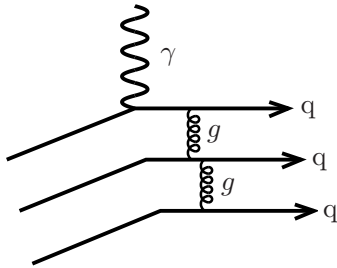


Fig. 3. Gluon ( $g$ ) exchanges among the constituent quarks ( $q$ ), to share the momentum transferred to the nucleon by the virtual photon.

Following the schematic representation in fig. 3, for the nucleons, that have three valence quarks, the minimum number of exchanges is two hence

$$F_i^N(q^2) \propto (-q^2)^{-1-i}, \quad q^2 \rightarrow -\infty,$$

formula, that in modulus squared reads  $|BW(s)|^2 = \left[ (M_j^2 - s)^2 + \Gamma_j^2 M_j^2 \right]^{-1}$ , the poles would be located exactly at  $M_j^2 \pm i\Gamma_j M_j$ .

with  $i=1,2$ .

The Pauli FF has a further power  $(-q^2)^{-1}$  since it is responsible for the spin-flip part of the nucleon electromagnetic current. The Sachs FFs, given in eq. (2), have the same behavior

$$G_{E,M}^N(q^2) \propto (-q^2)^{-2}, \quad q^2 \rightarrow -\infty.$$

The asymptotic behavior in the time-like region can be obtained by taking advantage from the analyticity and boundedness of FFs in the upper half plane,  $\text{Im}(q^2) > 0$ . Such regularities allow to apply the Phragmén-Lindelöf theorem [8], that ensures that FFs have the same vanishing power-law along any straight line from the origin to infinity, i.e.,

$$\lim_{|q^2| \rightarrow \infty} \frac{G_{E,M}^N(|q^2|e^{i\pi})}{G_{E,M}^N(|q^2|e^{i\theta})} = 1, \quad \forall \theta \in [0, \pi].$$

The identity between space-like and time-like asymptotic behavior is verified by taking this limit with  $\theta=0$ . It follows that

$$G_{E,M}^N(q^2) \propto (q^2)^{-2}, \quad q^2 \rightarrow \infty.$$

This result, since time-like FFs are complex, implies that imaginary parts vanish faster than the real ones

$$\lim_{q^2 \rightarrow \infty} \frac{\text{Im} [G_{E,M}^N(q^2)]}{\text{Re} [G_{E,M}^N(q^2)]} = \lim_{q^2 \rightarrow \infty} \arctan(\phi_{E,M}^N(q^2)) = 0,$$

i.e.,  $\Phi_{E(M)}(q^2)$ , the phase of the electric (magnetic) FF, tends to  $2\pi$  radians as stated by the Levinson theorem [9].

## 2 The threshold

The threshold region is represented by few hundreds MeV, say  $\delta E$ , interval  $(2M_N, 2M_N + \delta E)$ , which starts at the time-like  $N\bar{N}$  production energy. An  $e^+e^-$  collider operating at a CoM energy  $E \in (2M_N, 2M_N + \delta E)$  would produce  $N\bar{N}$  pairs almost at rest.

It is in this energy interval that charged nucleon and antinucleon experience the strongest electromagnetic interaction that, in the Born differential cross section formula of eq. (4), is accounted for by the Coulomb factor  $\mathcal{C}$ . The expression of  $\mathcal{C}$  can be obtained in the point-like limit as [10]

$$\mathcal{C} = |\psi_{\text{Coul.}}(0)|^2 = \frac{\pi\alpha}{\beta} \times \frac{1}{1 - e^{-\pi\alpha/\beta}} \equiv \mathcal{E} \times \mathcal{R}, \quad (5)$$

where  $\psi_{\text{Coul.}}(r)$  is the wave function solution of the Schrödinger equation with the Coulomb potential and  $\beta$

is the nucleon velocity given in eq. (4). The two terms  $\mathcal{E}$  and  $\mathcal{R}$ , called enhancement and resummation factor [11], account for the single and multi-photon contributions, respectively;  $\mathcal{E}$  dominates at threshold where  $\mathcal{R} \simeq 1$ , i.e.,

$$\mathcal{C} \simeq \mathcal{E} = \frac{\pi\alpha}{\beta}, \quad \beta \rightarrow 0^+.$$

The enhancement factor compensates for the closing of the phase-space by making the total Born cross section finite and different from zero at threshold, in particular [12]

$$\lim_{q^2 \rightarrow 4M_N^2} \sigma_{N\bar{N}}(q^2) = \frac{\pi^3 \alpha^2}{2M_N^2} |G^N(4M_N^2)|^2, \quad (6)$$

where  $G^N(4M_N^2)$  is the common threshold value of electric and magnetic FFs, that is, from the definitions of eq. (2), assuming no singularities for the Dirac and Pauli FFs,  $G_E^N(4M_N^2) = G_M^N(4M_N^2) \equiv G^N(4M_N^2)$ . It follows that, cross section and modulus of FFs can be measured even exactly at threshold. By taking advantage from the initial state radiation techniques, BaBar Collaboration measured  $p\bar{p}$  cross section [13], practically reaching the threshold.

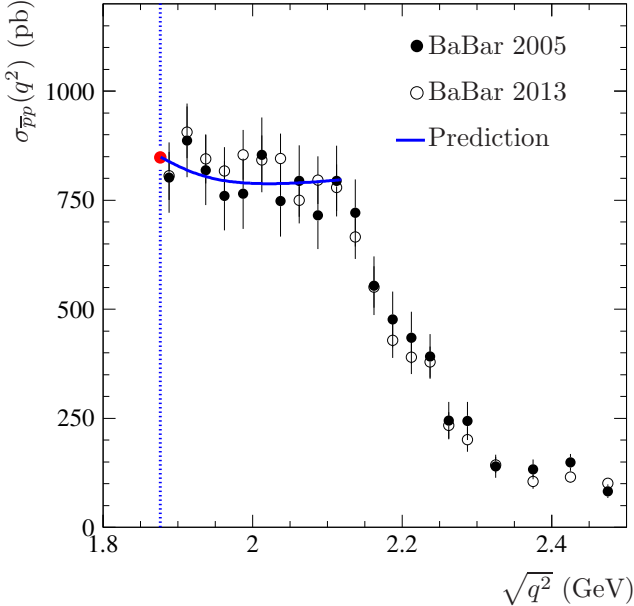


Fig. 4. Total cross section of  $e^+e^- \rightarrow p\bar{p}$ , measured by the BaBar Collaboration in 2005, solid circles, and 2012, empty circles. The blue dashed line indicates the physical threshold  $\sqrt{q^2} = 2M_p$ . The solid red point at threshold represents the cross section expected if  $|G_E^p(4M_p^2)| = |G_M^p(4M_p^2)| = |G^p(4M_p^2)| = 1$ . The blue curve is a prediction, see text.

Solid and empty black circles in fig. 4 represent two sets of BaBar data [13] on  $e^+e^- \rightarrow p\bar{p}$  cross section, while

the red point at the production threshold, which is indicated by the blue dashed line, is the expected value for the total cross section in case of

$$|G_E^p(4M_p^2)| = |G_M^p(4M_p^2)| = |G^p(4M_p^2)| = 1.$$

In other words, assuming a flat cross section in the threshold region, BaBar Collaboration has measured, for the first time and at a percent level, a **unit FF at threshold**. Such a result seems to suggest that the physical threshold has a special meaning for the FFs, in contrast with their basic theoretical properties. Indeed, by considering a FF as the superposition of intermediate resonances and multi-hadron states, at these time-like four-momenta its value should be the sum of tails of these contributions, hence there is no reason for expecting this sum to be exactly one.

The flat  $e^+e^- \rightarrow p\bar{p}$  cross section in the threshold region could be explained by considering:

- FFs almost constant and unitary;
- a resummation factor which accounts for multi-gluon exchanges ( $\alpha \rightarrow \alpha_s$ )

$$\mathcal{R} \rightarrow \mathcal{R}_s = \frac{1}{1 - e^{-\pi\alpha_s/\beta}}, \quad \alpha_s = 0.5.$$

In fact, in this case, the total cross section, that is obtained from the expression of eq. (4) where all constants are reported in units of pb, becomes

$$\sigma_{p\bar{p}}(q^2) = [850 \text{ pb}] \frac{1}{\tau} \mathcal{R}_s,$$

and its behavior, shown as a blue curve in fig. 4, describes quite well the data.

On the other hand, the effective FF

$$G_{\text{eff}}(q^2) = \sqrt{\frac{1}{\mathcal{R}} \frac{\sigma_{p\bar{p}}(q^2)}{\mathcal{E} \frac{4\pi\alpha^2\beta}{3q^2} (1 + \frac{1}{2\tau})}},$$

extracted from the BaBar cross section data, by considering the usual resummation factor (eq. (5)), and reported in fig. 5, shows a steep decreasing behavior starting from the threshold, that, having a flat cross section, turns out to be

$$G_{\text{eff}}(q^2) \simeq \frac{1}{\sqrt{\mathcal{R}}} = \sqrt{1 - e^{-\pi\alpha/\beta}}, \quad \sqrt{q^2} \in [2M_p, 2M_p + \delta E].$$

The curve  $1/\sqrt{\mathcal{R}}$  is shown in red in fig. 5. It is in perfect agreement with the BaBar data on  $G_{\text{eff}}(q^2)$ , represented by black circles jointed by lines.

## 2.1 Isotropy at the $p\bar{p}$ production threshold

The identity of electric and magnetic FFs at the threshold is also interpreted as a consequence of isotropy.

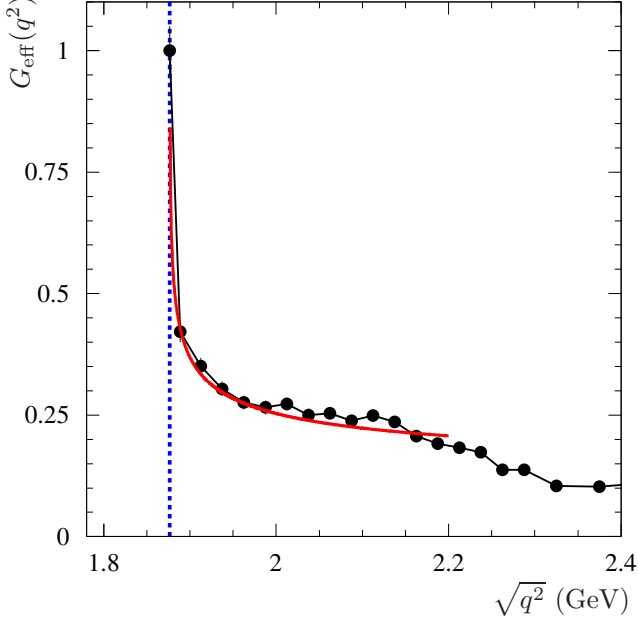


Fig. 5. The black circles, but for the point at the threshold, which has been obtained by extrapolating the cross section, are the data on the effective proton FF measured by the BaBar Collaboration. The red solid curve represents the function  $1/\sqrt{R}$ , see text. The dashed blue line indicates the proton physical threshold.

Besides Sachs and, Dirac and Pauli FFs, also partial wave FFs can be defined. From parity and total angular momentum conservation, in Born approximation,  $N\bar{N}$  can be produced with only two values of orbital angular momentum, i.e.,  $L_{N\bar{N}} = 0, 1$ . In fact, the  $N\bar{N}$  system has to have parity  $P_{N\bar{N}} = P_\gamma = -1$  and total angular momentum  $J_{N\bar{N}} = J_\gamma = 1$ , where  $P_\gamma$  and  $J_\gamma$  are photon quantum numbers. Since,  $P_{N\bar{N}} = (-1)^{L_{N\bar{N}}+1}$ ,  $-1$  is the intrinsic  $N\bar{N}$  parity, and the total spin is  $S_{N\bar{N}} = 0, 1$ , it follows that:  $L_{N\bar{N}}$  must be even ( $L_{N\bar{N}} = 0, 2, \dots$ ) and

$$J_{N\bar{N}} = 1 \in \{|L_{N\bar{N}} - S_{N\bar{N}}|, \dots, |L_{N\bar{N}} + S_{N\bar{N}}|\},$$

$$= \begin{cases} \{1\} & (L_{N\bar{N}}, S_{N\bar{N}}) = (0, 1) \\ \{1, 2, 3\} & (L_{N\bar{N}}, S_{N\bar{N}}) = (2, 1) \end{cases},$$

all the other combinations  $(L_{N\bar{N}}, S_{N\bar{N}})$  give total angular momenta different from  $J_\gamma = 1$ . Hence only S and D waves are allowed, the corresponding FFs are

$$G_S^N(q^2) = \frac{1}{3} \left( 2\sqrt{\tau} G_M^N(q^2) + G_E^N(q^2) \right),$$

$$G_D^N(q^2) = \frac{1}{3} \left( \sqrt{\tau} G_M^N(q^2) - G_E^N(q^2) \right),$$
(7)

while the total annihilation cross section in CoM and in terms of  $G_S^N$  and  $G_D^N$  reads

$$\sigma_{N\bar{N}}(q^2) = \frac{2\pi\alpha^2\beta}{q^2} \frac{1}{\tau} \left[ \mathcal{C} |G_S^N(q^2)|^2 + 2|G_D^N(q^2)|^2 \right],$$

where the Coulomb correction acts only on the S-wave term. From the definitions of eq. (7) follows that the isotropy at threshold, i.e., the presence at threshold of the only S wave and the vanishing of the D-wave contribution, is equivalent to the identity  $G_E^N(q_1^2) = G_M^N(q_1^2)$ .

Such an identity is experimentally observable, especially for lambda and sigma baryons, in a typical experiment at an  $e^+e^-$  collider (e.g. BESIII at BEPCII [14]). In particular, the ratio  $|G_E^B(q_1^2)/G_M^B(q_1^2)|$  is measurable, even exactly at the production threshold, for all those  $B\bar{B}$  final states where the (lambda or sigma) baryon,  $B$  (anti-baryon  $\bar{B}$ ), at rest in the Lab, decays weakly in a nucleon (anti-nucleon) and a pion, that have enough momentum to reach the detector.

Measuring a non-vanishing D-wave contribution, i.e., the inequality  $|G_E^B(q_1^2)/G_M^B(q_1^2)| \neq 1$  would be the first observation of the analyticity-violation for the Dirac and Pauli FFs, that must have a simple pole at threshold ( $\tau = 1$ ) with opposite residues. In more detail, we define

$$F_1^B(q^2) = \frac{-\Delta G^B}{\tau - 1} + F_{1,\text{an}}^B(q^2),$$

$$F_2^B(q^2) = \frac{\Delta G^B}{\tau - 1} + F_{2,\text{an}}^B(q^2),$$

where  $\Delta G^B = G_E^B(q_1^2) - G_M^B(q_1^2)$  and  $F_{1(2),\text{an}}(q^2)$  is the analytic part of the Dirac (Pauli) FF. In this case, i.e., by allowing for different values of Sachs FFs at threshold and assuming  $|\Delta G^B| \ll |G_M^B(q_1^2)|$ , the annihilation differential cross section of eq. (4) has the limit

$$\frac{d\sigma_{B\bar{B}}}{d\Omega} \xrightarrow{q^2 \rightarrow q_1^2} \frac{\alpha^2\beta}{3M_B^2} \left[ |G_M^B(q_1^2)|^2 + \text{Re}(\Delta G^B G_M^{B*}(q_1^2)) \sin^2(\theta) \right].$$

It depends on the scattering angle, and hence is not isotropic, even at threshold. This can be also seen by considering the values of the partial wave FFs at  $q^2 = q_1^2$ , they are

$$G_S^B(q^2) \xrightarrow{q^2 \rightarrow q_1^2} G_M^B(q_1^2) + \frac{\Delta G^B}{3}$$

$$G_D^B(q^2) \xrightarrow{q^2 \rightarrow q_1^2} -\frac{\Delta G^B}{3}.$$

As expected, the anisotropy, which is measured by the threshold value of  $G_D^B$ , depends on difference between electric and magnetic FFs.

Unique sources of anisotropy are corrections due to  $B\bar{B}$  final state interaction, that provide an overall power of  $\beta^{-2}$ , which means a simple pole for the FFs. Theoretical calculations give an order- $\alpha^2$  [15] effect in case of only Coulomb final state interaction (charged baryons). On the other hand strong Coulomb-like interaction, computed in case of heavy quarks [16], provides a large effect but proportional to  $\beta^n$  ( $n \in \mathbb{N}$ ), hence vanishing at threshold.

### 3 Conclusion

The threshold region for baryon FFs is a mine of information on low-energy strong dynamics as much rich as unexplored. Recently, in the  $p\bar{p}$  final state, a FF oscillatory behavior has been clearly identified [17] and in-

terpreted as a manifestation of  $p\bar{p}$  final state interaction. Moreover, the observation of anisotropy, by measuring a value different from one for ratio between the moduli of Sachs FFs, is now suitable for experiments like BES-III [14]. Indeed, in such an experiment the detection efficiency for a  $B\bar{B}$  pair of lambda or sigma baryons, is different from zero even exactly at threshold, when  $B\bar{B}$  are produced at rest in Lab, since the decay products have always enough momentum to reach the detector. From the theoretical point of view shading light on the threshold behavior would help in understanding, not only the nature of possible  $B\bar{B}$  final state corrections still underestimated or neglected, but also the unexpected unitary normalization observed in case of  $p\bar{p}$  and that seems to hold also for other  $B\bar{B}$  channels [18].

### References

- 1 S. Pacetti, R. Baldini Ferroli and E. Tomasi-Gustafsson, Phys. Rept. **550-551** (2015) 1.
- 2 R. G. Sachs, Phys. Rev. **126** (1962) 2256.
- 3 M. N. Rosenbluth, Phys. Rev. **79** (1950) 615.
- 4 A. Zichichi, S. Berman, N. Cabibbo, R. Gatto, Nuovo Cim. **24** (1962) 170.
- 5 A. Akhiezer, M. Rekalov, Sov. Phys. Dokl. **13** (1968) 572; A. Akhiezer, M. Rekalov, Sov. J. Part. Nucl. **4** (1974) 277.
- 6 A. Z. Dubnickova, S. Dubnicka and M. P. Rekalov, Nuovo Cim. A **109** (1996) 241.
- 7 V. Matveev, R. Muradyan, A. Tavkhelidze, Teor. Mat. Fiz. **15** (1973) 332; S. J. Brodsky, G. R. Farrar, Phys. Rev. Lett. **31** (1973) 1153.
- 8 E. Titchmarsh, *The Theory of Functions*, Oxford science publications, Oxford University Press, 1939.
- 9 N. Levinson, Danske Vid. Selsk. Math. Fys. Medd. **25**(9) (1949) 1.
- 10 A. D. Sakharov, Zh. Eksp. Teor. Fiz. **18** (1948) 631 [Sov. Phys. Usp. **34** (1991) 375]; A. Sommerfeld, *Atombau und Spektrallinien* (Vieweg, Braunschweig, 1944), Vol. 2, p. 130.
- 11 R. Baldini Ferroli, S. Pacetti and A. Zallo, Eur. Phys. J. A **48** (2012) 33.
- 12 R. Baldini, S. Pacetti, A. Zallo and A. Zichichi, Eur. Phys. J. A **39** (2009) 315.
- 13 B. Aubert *et al.* [BaBar Collaboration], Phys. Rev. D **73** (2006) 012005; J. P. Lees *et al.* [BaBar Collaboration], Phys. Rev. D **87** (2013) 9, 092005.
- 14 D. M. Asner *et al.*, Int. J. Mod. Phys. A **24** (2009) S1.
- 15 V. F. Dmitriev and A. I. Milstein, Phys. Lett. B **722** (2013) 83.
- 16 S. J. Brodsky, A. H. Hoang, J. H. Kuhn and T. Teubner, Phys. Lett. B **359** (1995) 355
- 17 A. Bianconi and E. Tomasi-Gustafsson, Phys. Rev. Lett. **114** (2015) 23, 232301.
- 18 R. Baldini Ferroli and S. Pacetti, Nucl. Phys. Proc. Suppl. **225-227** (2012) 211.